ACS APPLIED MATERIALS & INTERFACES

Research Article

www.acsami.org

Enhanced Photoluminescence in Au-Embedded ITO Nanowires

Hyunsu Kim, Sunghoon Park, Changhyun Jin, and Chongmu Lee*

Department of Materials Science and Engineering, Inha University, 253 Yonghyeon-dong, Incheon 402-751, Republic of Korea

Supporting Information

ABSTRACT: Gold (Au)-embedded indium tin oxide (ITO) nanowires were synthesized by thermal evaporation of a mixture of In_2O_3, SnO_2 and graphite powders on Si (100) substrates coated with Au thin films followed by annealing. At the initial stages of annealing, Au formed a continuous linear core located along the long axis of each ITO nanowire. The morphology of the Au core changed from a continuous line to a discrete line, and then to a droplet-like chain, finally evolving into a peapod in which crystalline Au nanoparticles were encapsulated in crystalline ITO with increasing annealing temperature. The ITO nanowires with the Au core showed an emission band at ~380 nm in the ultraviolet region. The ultraviolet emission intensity increased rapidly with increasing annealing temperature. The intensity of emission from the Au-peapod ITO nanowires (annealed at 750 °C) was approximately 20 times higher than that of the emission from the Au-core/ITO-shell ITO nanowires with a continuous linear shaped-Au core (annealed at 550 °C). This ultraintense ultraviolet emission might have originated mainly from the enhanced crystalline quality of the annealed ITO nanowires.

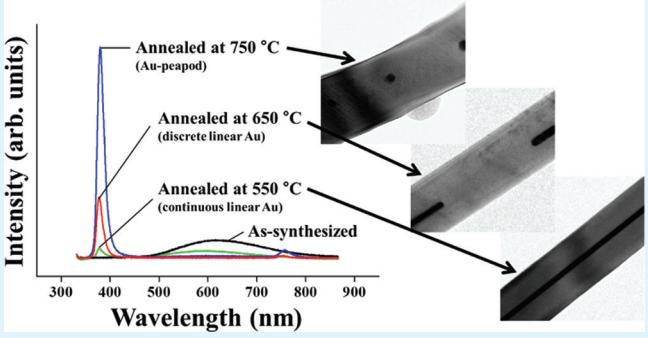

KEYWORDS: *Sn-doped In_2O_3 nanowires, gold-peapodded indium tin oxide (ITO), photoluminescence, thermal annealing*

INTRODUCTION

Tin-doped indium oxide, i.e., indium tin oxide (ITO), thin films have long been a focus of intensive research because of their excellent electrical conductivity and optical transparency, which are a core requirement for a good transparent conductor.[1] On the other hand, one-dimensional nanostructures, such as nanowires, nanorods, nanobelts, nanoribbons, nanoneedles, and nanotubes, have great potential because of their unique electrical and optical properties associated with the high aspect ratio and good crystallinity.[2−4] In particular, ITO nanowires have the advantages of being highly transparent and conducting over other material nanowires. Indeed, the development of light emitting devices with excellent performance using ITO nanowires as a transparent top contact has been reported.[5] The successful synthesis of ITO nanostructures with good performance by physical vapor deposition[1,6,7] has also been reported. ITO nanowires are expected to have widespread applications in nanoscale optoelectronic device fabrication.

In recent years, noble metal nanoparticles embedded in a dielectric material, known as a "peapod", have attracted considerable attention owing to their fascinating optical and electrical properties. Metal-dielectric nanocomposites show a nonlinear and fast optical response near the surface plasmon resonance (SPR) frequency because of their enhanced third-order optical susceptibility.[8−13] This property makes them suitable for optical switching devices and biosensors. This paper demonstrates that a combination of these interesting nanostructures with ITO nanowires can be applied to the fabrication of light emitting devices as well as optical switching devices and biosensors because of the giant enhancement of their luminescence. This paper reports the preparation of crystalline gold (Au) nanoparticles encapsulated periodically in cubic single-crystalline ITO nanowires and their enhanced photoluminescence properties. The results showed that ultraintense ultraviolet emission could be obtained from the Au-core/ITO-shell nanowires annealed at 750 °C.

EXPERIMENTAL SECTION

ITO nanowires were fabricated in a horizontal three zone tube furnace via a vapor−liquid−solid (VLS) mechanism. In_2O_3, Sn_2O_3, and graphite powders with a ratio of 4:1:1 were mixed together and placed into an alumina crucible positioned in the high temperature zone (950 °C). The quartz tube was purged with Ar gas flowing at 100 standard cubic centimeter per minute (sccm). Silicon (100) substrates coated with 4 nm thick Au thin films were placed in the low temperature region where the temperature was set to 850 °C. After the set temperature was reached, Ar and O_2 gases were introduced at flow rates of 95 and 5 sccm, respectively. The growth at the set temperature was continued for 35 min while the pressure was fixed to approximately 1 Torr. After cooling, a white layer of the deposits was found on top of the silicon substrate. For the second stage, annealing was conducted on the ITO nanowire samples to make the Au-core/ITO-shell or Au-embedded ITO nanowires. Ar gas (100 sccm) was introduced into the chamber. The chamber pressure was maintained

Received: August 16, 2011
Accepted: November 16, 2011
Published: November 16, 2011

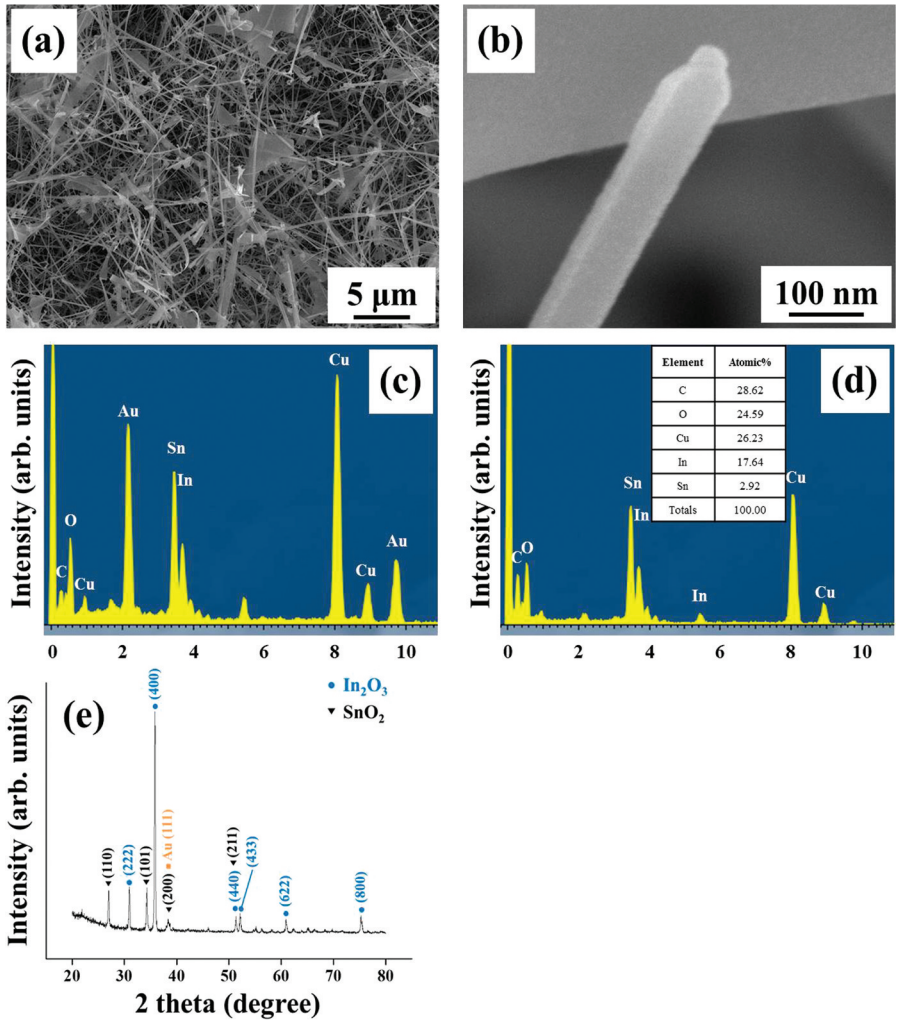

Figure 1. (a) SEM image of Au-core/ITO-shell nanowires. (b) Enlarged SEM image of a typical Au-core/ITO-shell nanowire. (c) EDX spectra of the particle at the tip of a typical Au-core/ITO-shell. (d) EDX spectra of the central part of the as-synthesized Au-core/ITO-shell nanowires. (e) XRD patterns of the Au-core/ITO-shell nanowires annealed at 650 °C.

at 1 Torr and the substrate temperature was maintained at 550, 650, or 750 °C for 1 h.

The products were characterized by glancing angle (0.5°) X-ray diffraction (XRD, X'pert MPD-Philips with Cu−K_α radiation), scanning electron microscopy (SEM, Hitachi S-4200), and transmission electron microscopy (TEM, Phillips CM-200) equipped with an energy-dispersive X-ray spectrometer (EDXS). High resolution TEM (HRTEM) images and selected area electron diffraction (SAED) patterns were also taken. The photoluminescence measurements were carried out at room temperature using a continuous wave He−Cd laser (wavelength, 325 nm; power, 100 mW) as the excitation source.

RESULTS AND DISCUSSION

Figure 1a shows the high-density Au-embedded ITO nanowires synthesized via a vapor−liquid−solid (VLS) mechanism. High-density ITO nanowires with a fairly uniform diameter were obtained. The typical diameter and length of the composite nanowires were a few tens of nanometers and a few tens to a few hundreds of micrometers, respectively. An Au particle with a different diameter from that of the other parts was observed at the tip of every nanowire, as shown Figure 1b. The EDX spectra (Figure 1c) taken at the tip of the nanowire show elemental Au as well as In, Sn, and O, which were also detected in other parts of the nanowire (Figure 1d). The Cu and C in the spectra were attributed to the TEM grid. The fact that the nanowires were quite uniform in diameter and had Au nanoparticles at their tips prove that they had grown through a VLS mechanism. Figure 1e shows the glancing-angle XRD pattern of the Au/ITO composite nanowires annealed in an Ar atmosphere at 550 °C for 1 h with the contribution of the Si substrate minimized. Besides an Au-related peak, the reflection peaks were readily indexed to the body-centered cubic (bcc) structure of In_2O_3 with lattice constants of a = 1.011 nm (JCPDS 06−0416) and the tetragonal structure of SnO_2 with lattice constants of a = 0.4738 nm, c = 0.3187 nm (JCPDS 41−1445). This indicates that the nanorods consist of crystalline indium tin oxide (ITO). The pattern exhibits the (222), (400), (440), (433), (622), and (800) reflections from In_2O_3, the (110), (101), (200), and (211) reflections from SnO_2 as well as the (111) reflection from Au.

Figures 2a-d show low-magnification TEM images of the Au-embedded ITO nanowires. Comparison of the TEM images indicates that the morphology of the Au core depends strongly on the annealing temperature. The Au core tends to change from a continuous linear shape to a discrete linear one and then finally to a droplet chainlike shape with increasing annealing temperature from 550 to 750 °C. Less Au is visible in the peapod structure compared to the cylindrical core in the TEM images. It is not clear at present, but we surmise that the rest of

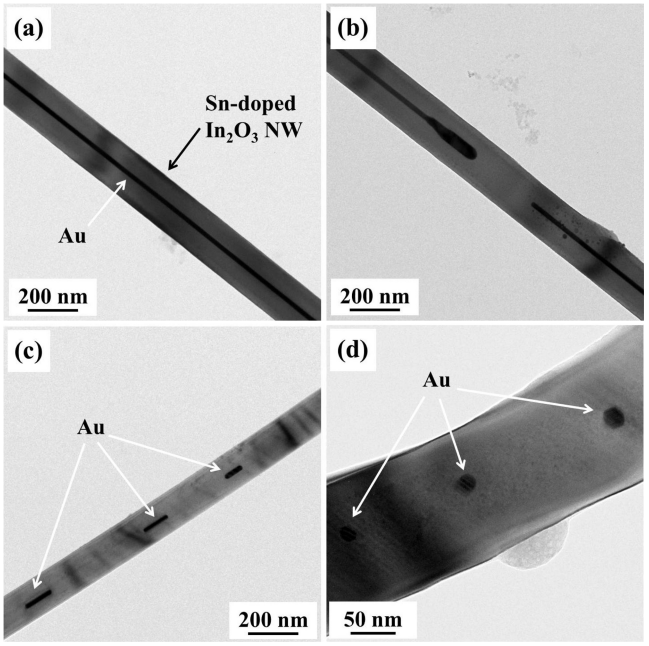

Figure 2. Low-magnification TEM image of the Au-core/ITO-shell nanowires: (a) as-synthesized, (b) annealed at 550 °C for 1 h, (c) annealed at 650 °C for 1 h, and (d) annealed at 750 °C for 1 h.

the Au has been dissolved into the ITO shell as impurities. The driving force for the instability of a cylindrical nanowire under the influence of capillarity or surface tension is the chemical potential gradient induced perturbation in the nanowire radius.[14] EDXS elemental maps (Figure 3a) display the

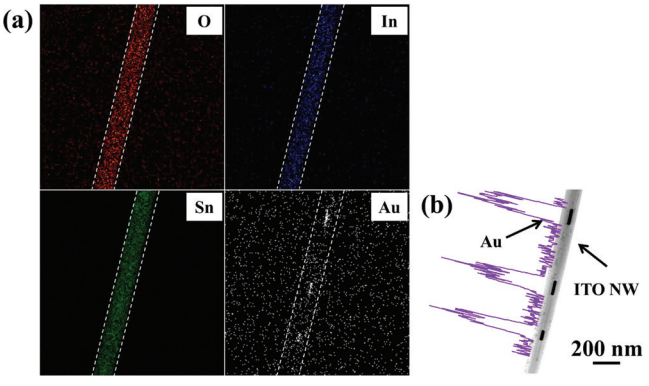

Figure 3. (a) EDX elemental maps of In, Sn, O, and Au elements and (b) EDX concentration profiles of elemental Au in a typical Au-core/ITO-shell nanowire along a line drawn along the long axis of the nanowire annealed at 650 °C for 1 h.

distribution of O (red), In (blue), Sn (green), and Au (white) in a typical Au-ITO composite nanowire obtained by annealing at 650 °C. The maps demonstrate that a discrete linear core mostly contains Au, whereas the other part (the shell region) of the nanowire is composed of In, Sn and O. The EDXS Au concentration profile along the long axis of the discrete linear core (Figure 3b) also shows that the Au concentration in the longish nanoparticles is by far higher than the other parts of the nanowire.

Figure 4a, b present, respectively, the local high-resolution TEM (HRTEM) images enlarging the ITO shell and Au core region in a typical nanowire. The resolved spacing between two

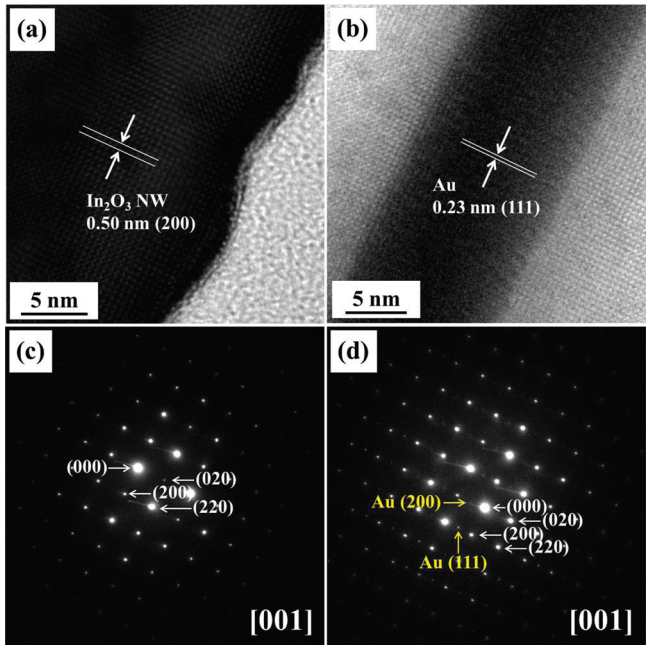

Figure 4. HRTEM images of (a) ITO shell region, (b) Au core region of a typical Au-embedded ITO nanowire, (c) SAED patterns of the ITO shell region, and (d) Au core region of a typical Au-embedded ITO nanowire.

neighboring parallel fringes in the shell region corresponding to the bcc In_2O_3 (200) plane was approximately 0.50 nm, and that between the two parallel neighboring fringes in the core region corresponding to the face-centered cubic Au (111) plane was approximately 0.23 nm (see the Supporting Information). The selected area electron diffraction (SAED) pattern corresponding to the ITO shell region (Figure 4c), which was recorded perpendicular to the long axis of the ITO nanowire, was indexed to the [001] zone axis of In_2O_3. The strong reflection spots in the corresponding selected area electron diffraction (SAED) pattern (Figure 4c) were assigned to the (200) and (020) reflections of bcc In_2O_3, indicating that the ITO nanowire in the TEM image is a single crystal. On the other hand, the dim spotty pattern of Au was overlapped on the strong spotty pattern of In_2O_3 in the SAED (Figure 4d) corresponding to the Au core. The strain in an annealed nanowire sample can be examined by checking the change in bond length in SAED, i.e., by comparing the bond length of the atoms in the annealed nanowires with that in the as-synthesized ones. A close comparison of the SAED patterns revealed that ITO nanowires or Au cores were not nearly strained because almost no difference is observed in the bond length in the SAED pattern between the core−shell nanowires annealed at 750 °C and as-synthesized ones.

Figure 5 shows the normalized room-temperature PL spectra of the ITO nanowires annealed at different temperatures for 1 h, i.e., the Au-core/ITO-shell nanowires along with that of as-synthesized ITO nanowires. The as-synthesized nanowires showed a weak broad emission band centered at approximately 610 nm, which is in good agreement with the emission band of the In_2O_3 nanowires reported previously. Mazzera et al.[14] reported that the PL spectrum of In_2O_3 nanowires at a low temperature (19 K) was composed of a broad band centered at approximately at 630 nm and a structured band at approximately 420 nm. The band at 630 nm was shifted to ~580 nm and the band at ~420 nm has disappeared with increasing the temperature from 19 to 300 K. Gao et al.[15]

dx.doi.org/10.1021/am201098e | ACS Appl. Mater. Interfaces 2011, 3, 4677–4681

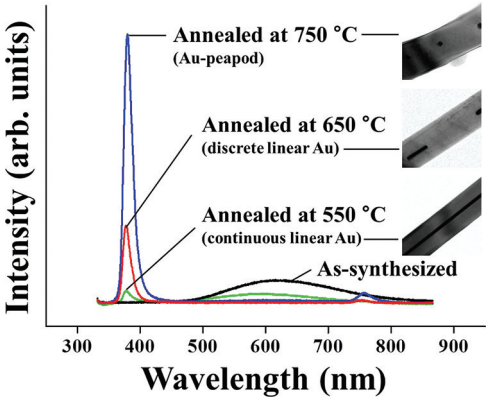

Figure 5. Room-temperature PL spectra of the as-synthesized and annealed Au-core/ITO-shell nanowires.

reported that ITO nanowires exhibited an emission band at ~430 nm whereas undoped In_2O_3 nanowires had an emission band at ~590 nm. The violet emission from the ITO nanowires may be due to a new defect generated by the Sn doping. The recombination of the electrons from this new donor level with the holes photogenerated in the valence band might have resulted in the visible emission at ~430 nm.

On the other hand, no emission band was observed at ~430 nm but at ~610 nm for the as-synthesized ITO nanowires. The lack of the violet emission was presumably due to the very low Sn doping concentration (~ 2.92 at %, Figure 1d) in the ITO nanowires. In contrast to the as-synthesized ITO nanowires, the annealed ITO nanowires, i.e., Au-core/ITO-shell nanowires showed a new emission band near 380 nm. A similar phenomenon was reported by Lin et al.[16] in that Au nanoparticles showed an ultraviolet emission band at ~350 nm. They also demonstrated that the intensity of the emission at 350 nm from the Au nanoparticles could be greatly enhanced by the incorporation of the Au nanoparticles into SiO_2 nanoparticles due to second harmonic surface plasmon resonance.[16] The ultraviolet emission intensity tended to increase rapidly with increasing annealing temperature. As stated above, with increasing annealing temperature, the Au core tended to change from a continuous linear shape to a discrete linear one, and then finally to a droplet chainlike shape. The intensity of emission from the Au-peapod ITO nanowires (annealed at 750 °C) was approximately 20 times higher than that of the emission from the Au-core/ITO-shell ITO nanowires with a continuous linear shaped-Au core (annealed at 550 °C). At a glance, it looks as if the emission intensity depended strongly on the morphology and distribution of the Au in the ITO nanowires. However, this ultraviolet emission from the Au-core/ITO-shell nanowires does not originate from the Au cores but from the ITO shells because of the following two reasons:

(1) For spherical gold particles, the plasmon resonance is to be expected around 530 nm,[16] which would yield a second harmonic of 265 nm.

(2) Even if such an effect would occur, this would be a highly nonlinear effect of two-photon photoluminescence which only occurs under femtosecond pulsed illumination. Therefore, Plasmon resonance does not apply to the PL of the Au-core/ITO-shell nanowires in this study because a continuous wave He−Cd laser (325 nm) was used for exciting the nanowire samples in the PL measurement.

We performed the absorption measurement of the nanowire samples to examine the origin of the ultraintense UV emission from the Au-core/ITO-shell nanowires annealed at 750 °C. Figure 6 shows the absorption spectra for the four different

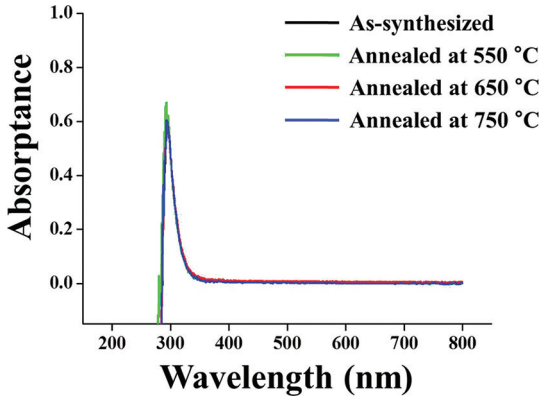

Figure 6. Absorption spectra of the as-synthesized and annealed Au-core/ITO-shell nanowires.

core−shell nanowire samples annealed at different temperatures. The spectra showed a major absorption peak at the same wavelength (~300 nm) despite the core−shell nanowires having different Au core morphologies. This result suggests that the ultraintense emission at 400 nm from the gold peapodded ITO nanowires does not originate from gold peapods but from the ITO shells. Furthermore, this absorption peak wavelength (~300 nm) is far from that of the Au nanoparticles (~530 nm) reported by Shi et al.[17] but closer to that of ITO (~280 nm) reported by Yu et al.[18] Therefore, we hypothesize that the enhancement of the emission at ~400 nm of the peapod nanowires in intensity originates from the ITO nanowires, not from the gold peapods. The fact that the energy value (~3.1 eV) corresponding to the wavelength of the ultraintense emission (~400 nm) from the gold peapodded ITO nanowires nearly the same as the ITO energy bandgap (3.5−4.5 eV)[19] supports the hypothesis. We may conclude that the 400 nm PL for the peapodded nanowires is attributed to the band-to-band transition of the ITO nanowires in the core−shell nanowires. Previous reports ascribed this UV emission to the near band edge transition wherein photogenerated holes near the valence band recombine with the electrons in the donor levels through a radiative process.[20−22] Such an efficient radiative process is often associated with a high crystalline quality or some quantum confinement effects.[20] Since the quantum confinement effect does not apply to the ITO nanowires with a mean diameter as large as ~180 nm which was synthesized in this study, the enhancement of the intensity of this UV emission might be mainly due to the enhanced crystalline quality of the as-synthesized ITO nanowires. It is widely accepted that the crystallinity of a thin crystalline material is enhanced by thermal annealing. The enhancement of the crystallinity of the ITO nanowires may, in turn, lead to the increase in the UV emission enhancement due to the suppression of nonradiative recombination centers in the ITO nanowires. The enhanced PL property of the Au-embedded ITO nanowires in a short-wavelength range is expected to find applications in the fabrication of nanosacle photonic and optoelectronic devices and compact photonic integrated circuits of high performance.

CONCLUSIONS

Au-core/ITO-shell nanowires synthesized by the thermal evaporation of a mixture of In_2O_3, SnO_2, and graphite powders on Au-coated Si (100) substrates thin films followed by annealing at 750 °C for 1 h showed ultraintense ultraviolet emission. The ultraviolet emission intensity increased rapidly with increasing annealing temperature, i.e., as the morphology of the Au core changed from a continuous line to a discrete line to a droplet chain. The intensity of the emission from the Au-peapod ITO nanowires (annealed at 750 °C) was approximately 20 times higher than that of the emission from the Au-core/ITO-shell ITO nanowires with a continuous linear shaped-Au core (annealed at 550 °C). The ultraintense ultraviolet emission might be due to the enhanced crystalline quality of the annealed ITO nanowires. Au-embedded ITO nanowires can find applications in the fabrication of nanosacle photonic and optoelectronic devices and compact photonic integrated circuits of high performance because of the great enhancement of their luminescence in addition to the applications in optical switching devices and biosensors.

ASSOCIATED CONTENT

Supporting Information

HRTEM image of a gold nanoparticle. This material is available free of charge via the Internet at http://pubs.acs.org/.

AUTHOR INFORMATION

Corresponding Author

*Tel.: +82 32 860 7536. Fax: +82 32 862 5546. E-mail: cmlee@inha.ac.kr (C. Lee).

ACKNOWLEDGMENTS

This study was supported financially by Korean Research Foundation (KRF) through the 2007 National Research Laboratory (NRL) Program.

REFERENCES

(1) Wan, Q.; Dattoli, E.; Fung, W.; Gao, W.; Chen, Y.; Pan, X.; Lu, W. *Nano Lett.* **2006**, *6*, 2909−2915.
(2) Huang, Y.; Duan, X.; Cui., Y.; Lauhon, L. J.; Kim, K.-H.; Lieber, C. M. *Science* **2001**, *294*, 1313−1317.
(3) Huang, M. H.; Mao, S.; Feick, H.; Yan, H.; Wu, Y.; Kind, H.; Weber, E.; Russo, R.; Yang, P. *Science* **2001**, *292*, 1897−1899.
(4) Iijima, S. *Nature* **1991**, *354*, 56−58.
(5) O'Dwyer, C.; Szachowicz, M.; Visimberga, G.; Lavayen, V.; Newcomb, S. B.; Torres, C. M. S. *Nat. Nanotechnol.* **2009**, *4*, 239−244.
(6) Wan, Q.; Wei, M.; Zhi, D.; MacManus-Driscoll, J. L.; Blamire, M. G. *Adv. Mater.* **2006**, *18*, 234−238.
(7) Nguyen, P.; Ng, H. T.; Kong, J.; Cassell, A. M.; Quinn, R.; Li, J.; Han, J.; McNeil, M.; Meyyappan, M. *Nano Lett.* **2003**, *3*, 925−928.
(8) Hu, M.-S.; Chen, H.-L.; Shen, C.-H.; Hong, L.-S.; Huang, B.-R.; Chen, K.-H.; Chen, L.-C. *Nat. Mater.* **2006**, *5*, 102−106.
(9) Hsieh, C.-H.; Chou, L.-J.; Lin, G.-R.; Bando, Y.; Goldberg, D. *Nano Lett.* **2008**, *8*, 3081−3085.
(10) Zhou, W. W.; Sun, L.; Xu, T.; Zhang, J. X.; Gong, H.; Fan, H. J. *Nanotechnology* **2009**, *20*, 455603.
(11) Chen, P.-H.; Hsieh, C.-H.; Chen, S.-Y.; Wu, C.-H.; Wu, Y.-J.; Chou, L.-J.; Chen, L.-J. *Nano Lett.* **2010**, *10*, 3267−3271.
(12) Wu, Y.-J.; Hsieh, C.-H.; Chen, P.-H.; Li, J.-Y.; Chou, L.-J.; Chen, L.-J. *Acs Nano* **2010**, *4*, 1393−1398.
(13) Park, G.-S.; Kwon, H.; Lee, E. K.; Kim, S. K.; Lee, J. H.; Li, X. S.; Chung, J. G.; Heo, S.; Song, I. Y.; Lee, J. H.; Choi, B. L.; Kim, J. M. *Adv. Mater.* **2010**, *22*, 2421−2425.
(14) Mazzera, M.; Zha, M.; Calestani, D.; Zappettini, A.; Lazzarini, L.; Salviati, G.; Zanotti, L. *Nanotechnology* **2007**, *18*, 355707.
(15) Gao, J.; Chen, R.; Li, D. H.; Jiang, L.; Ye, J. C.; Ma, X. C.; Chen, X. D.; Xiong, Q. H.; Sun, H. D.; Wu, T. *Nanotechnology* **2011**, *22*, 195706.
(16) Lin, H. Y.; Chen, Y. F. *Appl. Phys. Lett.* **2006**, *88*, 101914.
(17) Shi, W.; Jiang, L. *J. Colloid Interface Sci.* **2009**, *340*, 291−297.
(18) Yu, D.; Wang, D.; Yu, W.; Qian, Y. *Mater. Lett.* **2003**, *58*, 84−87.
(19) Hambergend, I.; Granquist, C. G. *J. Appl. Phys.* **1986**, *60*, R123.
(20) Cao, H.; Qiu, X.; Liang, Y.; Zhu, Q. *Appl. Phys. Lett.* **2003**, *33*, 761−3.
(21) Chen, C.-J.; Xu, W.-L.; Chern, M.-Y. *Adv. Mater.* **2007**, *19*, 3012−5.
(22) Wei, Z. P.; Guo, D. L.; Liu, B.; Chen, R.; Wong, L. M.; YangW, F.; Wang, S. J.; Sun, H. D.; Wu, T. *Appl. Phys. Lett.* **2010**, *96*, 031902.